THE JOURNAL OF BIOLOGICAL CHEMISTRY VOL. 287, NO. 45, pp. 37824–37834, November 2, 2012

Dynamin2, Clathrin, and Lipid Rafts Mediate Endocytosis of the Apical Na/K/2Cl Cotransporter NKCC2 in Thick Ascending Limbs*

Received for publication, May 29, 2012, and in revised form, September 6, 2012 Published, JBC Papers in Press, September 12, 2012, DOI 10.1074/jbc.M112.386425

Gustavo R. Ares[‡1] **and Pablo A. Ortiz**[‡§2]

From the [‡]*Hypertension and Vascular Research Division, Department of Internal Medicine, Henry Ford Hospital and* [§]*Department of Physiology, Wayne State University, Detroit, Michigan 48202*

Background: Apical NKCC2 mediates NaCl reabsorption by the thick ascending limb.
Results: Inhibition of dynamin-2, clathrin and lipid raft-mediated endocytosis blunted NKCC2 endocytosis, increasing steady-state surface NKCC2 levels.
Conclusion: NKCC2 undergoes constitutive endocytosis in native thick ascending limbs via dynamin-2 and two endocytic pathways.
Significance: Endocytic pathways regulate steady-state surface NKCC2 in native thick ascending limbs. Impaired NKCC2 endocytosis may induce salt-sensitive hypertension.

Steady-state surface levels of the apical Na/K/2Cl cotransporter NKCC2 regulate NaCl reabsorption by epithelial cells of the renal thick ascending limb (THAL). We reported that constitutive endocytosis of NKCC2 controls NaCl absorption in native THALs; however, the pathways involved in NKCC2 endocytosis are unknown. We hypothesized that NKCC2 endocytosis at the apical surface depends on dynamin-2 and clathrin. Measurements of steady-state surface NKCC2 and the rate of NKCC2 endocytosis in freshly isolated rat THALs showed that inhibition of endogenous dynamin-2 with dynasore blunted NKCC2 endocytosis by 56 ± 11% and increased steady-state surface NKCC2 by 67 ± 27% ($p < 0.05$). Expression of the dominant negative Dyn2K44A in THALs slowed the rate of NKCC2 endocytosis by 38 ± 8% and increased steady-state surface NKCC2 by 37 ± 8%, without changing total NKCC2 expression. Inhibition of clathrin-mediated endocytosis with chlorpromazine blunted NKCC2 endocytosis by 54 ± 6%, while preventing clathrin from interacting with synaptojanin also blunted NKCC2 endocytosis by 52 ± 5%. Disruption of lipid rafts blunted NKCC2 endocytosis by 39 ± 4% and silencing caveolin-1 by 29 ± 4%. Simultaneous inhibition of clathrin- and lipid raft-mediated endocytosis completely blocked NKCC2 internalization. We concluded that dynamin-2, clathrin, and lipid rafts mediate NKCC2 endocytosis and maintain steady-state apical surface NKCC2 in native THALs. These are the first data identifying the endocytic pathway for apical NKCC2 endocytosis.

The thick ascending limb of the loop of Henle (THAL)[3] reabsorbs up to 30% of the renal salt load, which is necessary to maintain salt and fluid homeostasis (1). The main transport pathway for NaCl entering the THALs is mediated by Na/K/2Cl cotransporter NKCC2 (2), which is expressed in the apical membrane and subapical space of medullary and cortical THALs including the macula densa cells (3–5). In humans, mutations of NKCC2 cause Bartter's syndrome, a disorder characterized by salt wasting, dehydration, and hypotension (6, 7), while in animal models of salt-sensitive hypertension, NKCC2 activity is enhanced (8–14). Despite its importance, the molecular mechanisms that regulate NKCC2 in THALs are poorly understood.

We previously showed that apical NKCC2 levels are directly related to NaCl reabsorption by the THAL (15–18) and constitutive NKCC2 endocytosis at the plasma membrane requires cholesterol. After NKCC2 is internalized, a fraction of the retrieved pool is recycled back to the plasma membrane (16). Thus dynamic trafficking of NKCC2 is essential for maintenance of surface levels. Blockade of NKCC2 endocytosis induces NKCC2 accumulation at the cell surface, which enhances NaCl reabsorption (16). This suggests there is a direct link between NKCC2 endocytosis and the regulation of NaCl reabsorption by the THALs, emphasizing the importance of this trafficking pathway in renal ion transport.

While little is known about the proteins that control NKCC2 endocytosis in THALs, several different proteins and entry pathways are known to be involved in apical endocytosis in other epithelial cells. Dynamin-2 is a GTPase that plays a key role in the release of newly formed vesicles from the plasma membrane during endocytosis (19–22). In the renal nephron, dynamin-2 has been detected in the collecting duct but its localization and function in the THAL are not known (23). Because several apical transporters such as NHE3 (24), ENaC (25, 26), and aquaporin-2 (AQP-2) (27) are known to be internalized via a dynamin2-dependent process in cultured epithelial cells, it is possible that NKCC2 is internalized via dynamin-2 in THALs.

Our earlier study showed that depletion of membrane cholesterol with methyl-β-cyclodextrin (MβCD) inhibited NKCC2 internalization and increased steady-state surface NKCC2 in THALs (16). Since MβCD blocks clathrin-, caveolin-, and

* This work was supported, in whole or in part, by National Institutes of Health Grant R0–1 HL080409 (to P. A. O.).
[1] Supported in part by a Predoctoral Fellowship Grant 0715579Z from the American Heart Association.
[2] To whom correspondence should be addressed: Hypertension and Vascular Research Division, Department of Internal Medicine, Henry Ford Hospital, 2799 West Grand Blvd., Detroit, MI 48202. Tel.: 313-916-7164; Fax: 313-916-1479; E-mail: portiz1@hfhs.org.
[3] The abbreviations used are: THAL, thick ascending limb; MβCD, methyl-β-cyclodextrin; MesNa, sodium 2-mercaptoethanesulfonate; PS, perfusion solution; NKCC2, sodium, potassium, 2 chloride cotransporter.

clathrin/caveolae-independent endocytic pathways (28, 29), any of these may be involved in NKCC2 endocytosis. Clathrin-mediated endocytosis is one of the best studied endocytic pathways. Several accessory proteins control clathrin-coated pit formation and internalization (30). Apical transporters such as the Na^+/H^+ exchanger (NHE3) (31), epithelial Na^+ channel (ENaC) (25), cystic fibrosis transmembrane conductance regulator (CFTR) (32), and urea transporter (UT-A1) (33) are internalized via the clathrin-mediated pathway. In addition, biochemical studies indicate that a fraction of NKCC2 partitions into Triton X-100-resistant membrane domains (known as "lipid raft compartments") (34, 35); however, little is known about their role in mediating apical endocytosis in renal tissue. To our knowledge, there have been no direct studies examining the pathway for NKCC2 endocytosis. Here we tested the hypothesis that surface NKCC2 undergoes endocytosis via a dynamin-2, clathrin and lipid raft-dependent manner in native THALs.

EXPERIMENTAL PROCEDURES

Constructs, Adenoviruses, and Reagents—Full-length rat dynamin-2 and a single point mutation of lysine 44 to alanine (dyn2K44A) were kindly provided by Dr. Mark McNiven (Mayo Clinic, MN) and subcloned into a pAd5CMV plasmid to produce the adenoviruses. DNA constructs were verified by restriction enzyme digestion and sequencing. Recombinant replication-deficient adenoviruses containing eGFP (control) or a dominant negative dynamin-2 (dyn2K44A) mutant under control of the cytomegalovirus (CMV) promoter were generated and purified by Viraquest (North Liberty, IA). Caveolin-1 was silenced using adenoviruses carrying shRNA-Cav1 (kindly provided by Debbie C. Thurmond (Indiana University) (36–38). Dynasore, filipin III, and chlorpromazine were obtained from Sigma. Pitstop2 was obtained from Abcam Biochemicals (Cambridge, MA).

Physiological Solution—The composition of the physiological solution (PS) was (in mM): NaCl 130, NaH_2PO_4 2.5, KCl 4.0, $MgSO_4$ 1.2, L-alanine 6, Na-citrate 1.0, glucose 5.5, Ca-lactate 2.0, and HEPES 10; pH 7.40.

Animals—Suspensions of rat medullary THALs were obtained as described previously (15–18). Male Sprague-Dawley rats weighing 200–250 g (Charles River Breeding Laboratories, Wilmington, MA) were maintained on a diet containing 0.22% sodium and 1.1% potassium (Purina, Richmond, IN) with water *ad libitum*. All animal protocols were approved by the Institutional Animal Care and Use Committee (IACUC) of Henry Ford Hospital.

Measurement of Steady-state Surface NKCC2 in THALs—Suspensions of rat medullary THALs were obtained and steady-state surface NKCC2 was measured in suspensions of purified THALs as described previously (15–18).

Endocytosis of NKCC2 in THALs—NKCC2 retrieval from the apical surface was measured as described previously (16). Briefly, suspensions were pretreated with vehicle or inhibitor for 20 min at 37 °C. Then, THALs were cooled and surface proteins were biotinylated at 4 °C. Suspensions were maintained for 10 min. at 4 °C with vehicle or inhibitor before being warmed to 37 °C to allow endocytosis for 7.5, 15, or 30 min. Then the THALs were rapidly cooled by adding chilled PS to stop protein trafficking. THALs were treated for 30 min with the membrane-impermeant reducing agent MesNa (50 mM) in a reducing buffer (in mM: Hepes 50, $MgCl_2$ 1, NaCl 125, Tris-Cl 50, pH 8.0) to strip biotin from surface proteins by reducing the disulfide bridge in NHS-SS-biotin. Endocytosed biotinylated proteins were protected due to the low membrane permeability of MesNa. Excess MesNa was washed away and quenched with iodoacetamide (25 mM). THALs were lysed with buffer (in mM: 150 NaCl, 50 Tris-HCl, pH 7.4, 5 EDTA, 2% (v/v) Triton X-100, 0.2% (w/v) SDS, and protease inhibitors: 10 μg/ml aprotinin, 5 μg/ml leupeptin, 4 mmol/liter benzamidine, 5 μg/ml chymostatin, and 5 μg/ml pepstatin A (Sigma)). Equal amounts of proteins were incubated with streptavidin-agarose beads and the recovered endocytosed proteins, resolved by SDS-polyacrylamide gel electrophoresis. In each experiment a control biotinylated sample, (kept at 4 °C) was treated with MesNa to ensure complete stripping of surface biotin. MesNa effectively removed 97.6 ± 0.2% of biotin from surface NKCC2 ($n = 15$). The remaining signal was considered background and subtracted from other bands treated with MesNa (See Fig. 1*B*, *line 3*). The signal from bands showing internalized NKCC2 was expressed as a percentage of baseline surface NKCC2.

Endocytosis of Transferrin in THALs by Fluorescence Microscopy—To monitor clathrin-mediated endocytosis in THALs, we measured accumulation of fluorescence conjugated transferrin (Alexa-Fluor, 568 nm) by fluorescence microscopy as described previously (21, 39). THALs were equilibrated at 37 °C for 15 min in PS with 1% BSA (pH 7.4) containing vehicle or inhibitor. Then Alexa568-transferrin (10 μg/ml) was added to the bath for 30 min to allow internalization. The reaction was stopped by adding cold PS. THALs were washed once with PS to eliminate excess transferrin in solution and then with acid-wash (PS containing 1% BSA, pH: 3.5) to remove non-endocytosed surface bound transferrin. THALs were fixed with 4% paraformaldehyde (pH: 7.4), rehydrated with regular PS, and mounted on glass slides. Fluorescence images were acquired at 568 nm excitation using a scanning confocal microscopy system (Visitech International) mounted on an inverted Nikon TE2000-eclipse microscope, without a slit (non-confocal mode), and using a 60× lens. Fluorescence emissions were acquired, recorded and measured with a 590 nm LP filter. Regions of interest encompassing THALs were generated and the mean fluorescence intensity of 10–20 tubules per preparation was averaged. Data are expressed as arbitrary units (a.u.).

Recycling of NKCC2 in THALs—Recycling of NKCC2 was measured with a modified surface biotinylation protocol (16). First, surface NKCC2 was biotinylated in THAL suspensions at 4 °C as described above. One aliquot was kept at 4 °C to measure total surface NKCC2 levels. The rest of the THALs were warmed to 37 °C for 30 min to allow endocytic retrieval while gassing the bath solution every 5 min with 100% O_2, then rapidly cooled to 4 °C and maintained on ice. The remaining surface biotinylated NKCC2 was stripped at 4 °C with MesNa 50 mM as described for endocytosis, leaving only endocytosed proteins biotinylated. The THAL suspension was pre-incubated with vehicle or inhibitors for 10 min and then aliquots warmed to 37 °C for 0 (kept at 4 °C), 7.5, 15, or 30 min. To stop traffick-

ing, THALs were rapidly cooled to 4 °C. Surface biotinylated proteins that recycled back to the membrane were stripped with a second-round of MesNa 50 mM. Finally, THALs were treated with iodoacetamide (a reagent that eliminates the remaining MesNa from the bath) and lysed as described above. In every experiment, controls were performed to monitor baseline surface NKCC2, efficiency of MesNa stripping, and retrieved NKCC2 at 30 min (0-time point for recycling) which was set to 100%. We then calculated the percentage of retrieved NKCC2 that disappeared on the second round of stripping due to recycling.

In Vivo Gene Transfer of THALs—In vivo adenovirus-mediated gene transfer to the renal medulla was performed as described previously (40, 41). Rats were anesthetized, shaved, and cleaned. The left kidney was exposed via a flank incision, fatty tissue removed, and both the renal artery and vein clamped. Adenoviruses (1×10^{12} particles/ml) were loaded into PE50 tubing connected to a nanoliter syringe pump (Harvard Apparatus, Holliston, MA) set at 20 μl/min. A 30-gauge needle was attached to the other end of the tubing to inject the viruses into the renal outer medulla. The needle was inserted perpendicular to the renal capsule, parallel to the medullary rays and aimed toward the medulla. Five injections were made in 6 min (100 μl total volume), and the clamp was removed from the renal artery and vein after 8 min. After 6 to 7 days the left kidney was removed, and THALs isolated as described above. Similar to maximal eGFP expression after transduction (40), the maximal inhibitory effect of dyn2K44A occurred 7 days after viral injection (data not shown). Maximal inhibition of caveolin-1 expression occurred 4 days after renal transduction of Ad-shRNACav-1.

Western Blot—Proteins were eluted from streptavidin beads or THAL lysates by boiling (1 min) and then separated by centrifugation at 10,000 × *g*, loaded into each lane of a 6% SDS-polyacrylamide gel, separated by electrophoresis and transferred to Immobilon-P polyvinylidene difluoride membranes (PVDF) (Millipore, Bedford, MA). Membranes were blocked and blotted as described before (15). To detect dynamin-2, we used Hudy-1 antibody (42), caveolin-1 antibody (BD Transduction, San Jose, CA). Monoclonal anti-GAPDH (Chemicon, Temecula, CA) was used at 1/10,000 dilution. HRP-labeled secondary antibodies were detected by chemiluminescence and quantified by densitometry (15–18). Exposure time and amount of protein loaded were optimized so that optical densities were linear.

Localization of Internalized NKCC2 and Clathrin Heavy Chain in Isolated THALs—Two rounds of labeling were performed. First we labeled apical NKCC2 in isolated perfused THALs kept at 4 °C with an antibody directed toward an extracellular sequence located between TM3 and TM4 as described previously (15–18) added to the flowing apical bath. After washing, Alexa488-labeled anti-rabbit F′ab (Invitrogen, Carlsbad, CA) were added to the lumen at 4 °C for 20 min, then washed away and THALs warmed to 37 °C for 15 min to allow endocytosis. Next, THALs were cooled and the luminal solution replaced by PS containing 1% BSA, pH 3.5 (acid-wash) to remove the label from non-endocytosed surface NKCC2. Finally, THALs were fixed with 4% paraformaldehyde (*p*H 7.4) and blocked with 2.5% BSA, followed by labeling for 1 h with an anti-clathrin heavy chain mouse monoclonal antibody (BD Transduction, Franklin Lakes, NJ) followed by AlexaFluor 568 anti-mouse IgG highly cross-adsorbed at 1:200 in 2.5% BSA. Images were acquired using a laser scaning confocal microscopy system (Visitech, Sutherland, England) with Ar (488 nm) or Kr/Ar (568 nm) laser excitation controlled by an acousto-optic tunable filter. Images were acquired at 100× (1.3NA) and fluorescence observed with 525/55-nm BP or 590-nm LP filters, respectively. Image files were converted to the tagged image file format (TIFF), pseudocolored, and overlapped using Adobe Photoshop software.

Inhibition of Clathrin-mediated Endocytosis with PP19—Clathrin-mediated endocytosis requires the formation of a complex between clathrin, synaptojanin, amphiphysin, dynamin, and endophilin. The peptide VAPPARPAPPQRPPPPSGA (PP19) specifically blocks formation of this complex by preventing the SH3 domain of endophilin from interacting with synaptojanin (43–46), thereby inhibiting clathrin-mediated endocytosis. The peptides PP19 and PP19-FITC were synthesized by Genescript USA (Piscataway, NY). A Chariot intracellular peptide delivery system (Active Motif, Carlsbad, CA) was used to facilitate intracellular peptide delivery into THAL cells at the concentration recommended by the manufacturer. For this, Chariot reagent was dissolved in distilled water and the peptide PP19 (which has a theoretical molecular mass of 1860.13 g) was dissolved in regular PS. The peptide and Chariot solutions were mixed at a ratio of 1/10 (as recommended by the manufacturer) and kept at room temperature for 60 min to allow chariot-peptide complex to form. To confirm transduction of the peptide, we repeated the experiment using a FITC-labeled PP19 peptide and examined the accumulation of the peptide in THAL cells by fluorescence microscopy (Fig. 4*D*).

Statistics—Data are expressed as means ± S.E.. One-way ANOVA was used to determine statistical differences between means in different treatment groups when measuring surface and total NKCC2 by Western blot and fluorescence imaging. *, $p < 0.05$ was considered statistically significant. Error bars represent S.E.

RESULTS

Dynamin-dependent NKCC2 Endocytosis in THALs—We previously found that NKCC2 undergoes constitutive endocytosis in THALs, however, the proteins involved are unknown. We hypothesized that the GTPase dynamin-2 mediates NKCC2 retrieval in THALs. First, we studied dynamin-2 expression in THALs. A single band at the expected molecular weight of dynamin-2 (~100 kDa) was observed in THAL lysates by Western blot (Fig. 1*A*). Then we studied the role of dynamin in NKCC2 endocytosis using dynasore, a membrane-permeable inhibitor that blocks dynamin GTPase activity at concentrations between 50 and 100 μM (47, 48). THAL suspensions were pretreated with either vehicle or dynasore at 37 °C for 20 min, rapidly cooled to 4 °C and surface protein labeled with NHS-SS-biotin. Endocytosis of biotinylated NKCC2 was measured for 15 or 30 min in the presence of vehicle or dynasore. We first tested a range of dynasore concentrations (25, 50, and 100 μM) and found that 100 μM was most effective in blocking

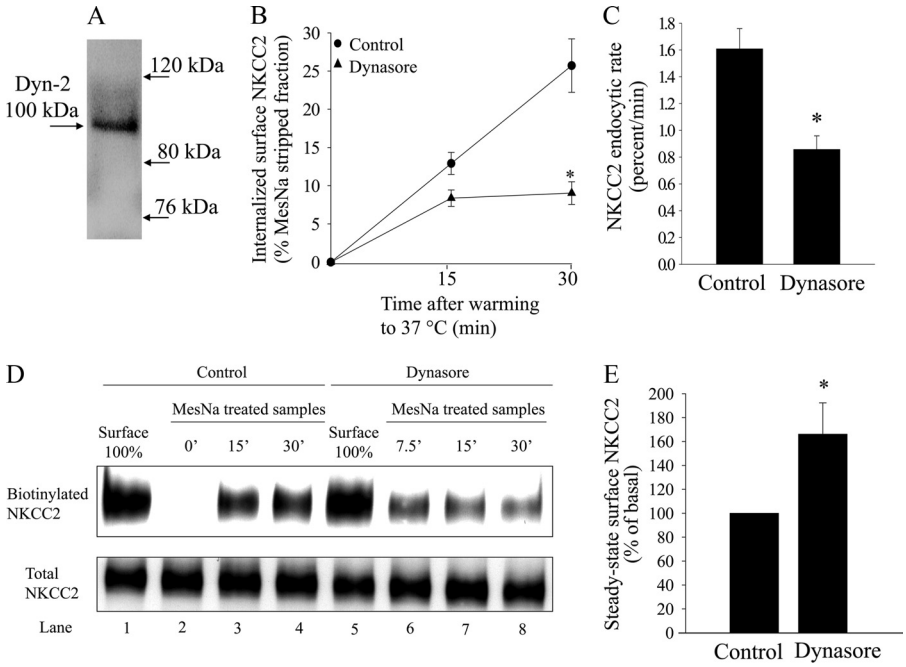

FIGURE 1. **Effect of dynamin inhibition on NKCC2 endocytosis in THALs.** *A*, representative Western blot showing dynamin-2 expression in rat medullary THALs at the expected molecular weight of ~100 kDa (lane loaded with 25 μg of THAL lysate). *B*, cumulative data showing the effect of vehicle (DMSO) or dynasore (100 μM) on constitutive NKCC2 endocytosis in THALs. THAL suspensions were incubated at 37 °C for 15 or 30 min in the absence (control, *circles*) or presence of 100 μM dynasore (*triangles*). Endocytosed NKCC2 was detected by Western blot as described in "Experimental Procedures" and mean optical density quantified by densitometry. Basal: 15 min = 13.0 ± 1.4%; 30 min = 25.7 ± 3.5%; dynasore: 15 min = 8.2 ± 1.0%, 30 min = 7.7 ± 1.1%; $n = 7$, *, $p < 0.05$). Data are expressed as a percentage of the MesNa-stripped fraction. Error bars represent S.E. *C*, quantification of NKCC2 trafficking rate, derived from the slopes of the data shown in *B*. Basal: 1.66 ± 0.21% per min; dynasore: 0.60 ± 0.10% per min: $n = 7$, *, $p < 0.05$. *D*, representative Western blot showing NKCC2 endocytosis in THALs treated with vehicle (DMSO) or dynasore (100 μM). In the *top panel*, *lanes 1* and *5* show expression of steady-state surface NKCC2 (basal surface NKCC2) treated with vehicle (DMSO) or dynasore (100 μM), respectively. *Lane 2* shows steady-state surface NKCC2 after treatment with the reducing agent MesNa (which efficiently strips biotin) compared with *lane 1*. After stripping, THALs were incubated for 0 min (*lane 2*), 15 min (*lane 3*), or 30 min (*lane 4*) under basal conditions and 7.5 (*lane 6*), 15 min (*lane 7*), or 30 min (*lane 8*) under dynasore treatment at 37 °C to allow protein trafficking. THALs were cooled and endocytosed NKCC2 (protected from MesNa) was precipitated, detected by Western blot, and measured by densitometry. The *lower panel* shows intracellular NKCC2 from each sample. *E*, cumulative data showing the effect of vehicle (DMSO) or dynasore (100 μM) on steady-state surface NKCC2 levels in THALs. Samples were treated for 20 min at 37 °C, then biotinylated as described in "Experimental Procedures"; surface NKCC2 was detected by Western blot and quantified by densitometry. Basal, 100%; dynasore (100 μM): 167 ± 27%; ($n = 6$, *, $p < 0.05$). Error bars represent S.E.

NKCC2 endocytosis after 30 min (baseline = 22.6 ± 1.8%; dynasore 25 μM = 19.3 ± 3.8%; dynasore 50 μM = 18.0 ± 2.4%; dynasore 100 μM = 14.0 ± 2.3%, $n = 3$; data not shown). Thus we used 100 μM dynasore to inhibit dynamin in THALs. When THALs were treated with dynasore at 100 μM, NKCC2 endocytosis was inhibited by 70% at 30 min, an average decrease in the rate of NKCC2 endocytosis of 56 ± 11% (Fig. 1, *B–D*), suggesting that dynamin activity is involved in NKCC2 endocytosis. Because NKCC2 undergoes constitutive trafficking into and out of the apical membrane, we expected selective inhibition of endocytosis would increase steady-state surface NKCC2 due to accumulation at the plasma membrane, and indeed 100 μM dynasore increased surface NKCC2 by 67 ± 27% (Fig. 1*E*).

The decrease in internalized biotinylated NKCC2 observed during dynamin inhibition is most likely caused by decreased endocytosis. However, this signal may also be decreased by enhanced NKCC2 recycling back to the surface. To assure this is not the case, we studied the effect of dynasore on NKCC2 recycling in native THALs as described previously (16). We found that dynasore did not stimulate NKCC2 recycling during 30 min, but rather tended to inhibit it (baseline: 44 ± 7%; dynasore: 35 ± 5% of internalized NKCC2 at 30 min; $n = 5$; n.s.). Thus, the inhibition of endocytosis caused by dynasore is not affected by recycling and is in part underestimated by a small inhibitory effect on recycling. Taken together, these data suggest that inhibition of dynamin decreases the rate of NKCC2 endocytosis and induces accumulation of NKCC2 at the cell surface.

In Vivo Expression of Dominant Negative Dynamin-2 (K44A) Decreases Constitutive NKCC2 Endocytosis in THALs—Dynasore inhibits all dynamin isoforms. To specifically study dynamin-2 mediated endocytosis, we expressed a dominant negative mutant of rat dynamin-2 (Dyn2K44A) in THALs. For this, we transduced THALs in the renal medulla with adenoviruses expressing eGFP (control) or Dyn2K44A as described previously (40, 41). THAL Dyn2K44A expression was confirmed by confocal fluorescence imaging of THALs 7 days after viral transduction. We found that in THALs transduced with Dyn2K44A, the average rate of NKCC2 endocytosis decreased by 38 ± 8% over a period of 30 min (Fig. 2, *A* and *B*). There was no significant change in the rate of NKCC2 endocytosis in THALs transduced with CMV-eGFP alone (control) compared with THALs obtained from non-transduced kidneys ($n = 5$, not shown). If NKCC2 endocytosis is inhibited by decreased dynamin-2 activity we would expect steady-state surface NKCC2 to increase due to accumulation at the plasma membrane, and indeed steady-state surface NKCC2 levels increased by 37 ± 8% in THALs transduced with Dyn2K44A (Fig. 2*C*)

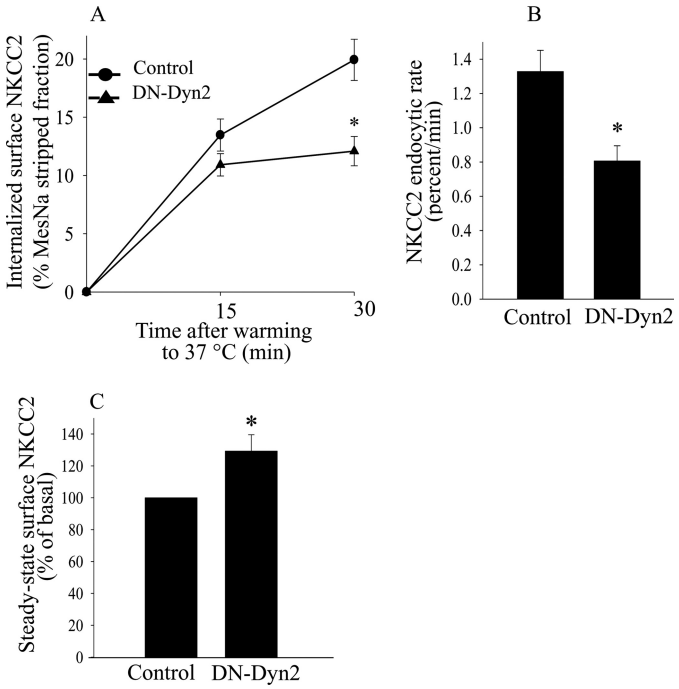

FIGURE 2. **Effect of dominant negative Dyn2(K44A) mutant on constitutive NKCC2 endocytosis in THALs.** *A*, cumulative data for constitutive NKCC2 endocytosis over time in THAL suspensions under basal conditions (*full line*) or after transduction with dominant negative rat Dyn2(K44A) (*dotted line*). *In vivo* adenovirus-mediated gene transfer of Dyn2(K44A) was performed as described in "Experimental Procedures." THALs from control or transduced kidneys were biotinylated and incubated at 37 °C for 15 or 30 min. (Basal 15 min, 13.5 ± 1.4%; 30 min, 19.9 ± 1.7%; Dyn2(K44A) 15 min, 10.9 ± 0.9%; 30 min, 12.1 ± 1.2%: $n = 6$, *, $p < 0.05$). Data are expressed as a percentage of the MesNa-stripped fraction. *B*, quantification of NKCC2 trafficking rate, derived from the slopes of the data shown in *A*. Basal: 1.33 ± 0.12% per min; Dyn2(K44A): 0.81 ± 0.09% per min; ($n = 6$, *, $p < 0.05$). Error bars represent S.E. *C*, cumulative data showing the effect of Dyn2(K44A) expression on steady-state surface NKCC2 levels in THALs. Dyn2(K44A) increased surface NKCC2 levels in THALs by 37 ± 8.3% ($n = 8$, *, $p < 0.05$).

whereas the total pool of NKCC2 did not change (basal, 100%; Dyn2K44A = 103 ± 6%; $n = 9$, data not shown). Transducing THALs with an adenovirus for CMV-eGFP (control) did not significantly affect steady-state surface NKCC2 nor the total pool of NKCC2 ($n = 7$, data not shown). We believe this is the first demonstration that dynamin-2 is involved in endocytosis in the native renal epithelium, and specifically NKCC2 internalization in THALs.

Inhibition of Clathrin-mediated Endocytosis Blunts NKCC2 Endocytosis in THALs—Dynamin-2 mediates both clathrin- and caveolin-mediated endocytosis. Since the endocytic pathway for NKCC2 has not been defined to our knowledge, we hypothesized that clathrin is involved in NKCC2 endocytosis. We studied the expression of clathrin heavy chain in THALs by confocal microscopy and found abundant expression of the clathrin heavy chain at the apical side and subapical space of THALs (Fig. 3*A*). Furthermore, we studied whether internalized NKCC2, labeled with an exofacial antibody co-localized with clathrin heavy chain in the sub-apical space. Co-localization of clathrin heavy chain and NKCC2 endocytosed from the apical membrane was observed in some small punctae and larger sub-apical structures in isolated THALs (Fig. 3*B*), suggesting that clathrin may be involved in NKCC2 retrieval. Therefore, we studied the effect of inhibiting clathrin-mediated endocytosis with the inhibitor chlorpromazine on NKCC2 retrieval. 20 μM chlorpromazine blunted the rate of NKCC2 endocytosis by 52 ± 10% (Fig. 4, *A* and *B*) without affecting the total NKCC2 pool in THALs. To confirm that chlorpromazine inhibits clathrin-mediated endocytosis, we monitored endocytosis of Alexa568-labeled transferrin in THALs for 30 min by fluorescence microscopy, and found that chlorpromazine blunted transferrin internalization by 42 ± 7% (Fig. 4*C*).

The decrease in internalized biotinylated NKCC2 caused by clathrin inhibitors is most likely caused by decreased endocytosis. However, it may be influenced by enhanced recycling back to the surface. To assure this is not the case, we studied the effect of chlorpromazine on constitutive NKCC2 recycling in native THALs (16). We found that chlorpromazine did not stimulate NKCC2 recycling, but rather inhibited it by 35 ± 11% (baseline-30 min: 30 ± 7%; chlorpromazine-30 min: 19 ± 4%; $n = 4$; *, $p < 0.05$). Thus, the inhibition of endocytosis caused by chlorpromazine is larger than measured, and the effect underestimated by a mild inhibitory action of this agent on NKCC2 recycling.

Clathrin-mediated endocytosis requires formation of a complex between clathrin, synaptojanin amphiphysin, dynamin, and endophilin (43, 44, 49). To test whether a clathrin-mediated pathway is involved in NKCC2 internalization, we used the peptide PP19 which specifically blocks the interaction between clathrin and its adaptor proteins, thereby inhibiting the formation of clathrin coated vesicles (44, 45). We found that inhibition of clathrin-mediated endocytosis with PP19 at 6 μM blunted the rate of NKCC2 endocytosis by 52 ± 5% (Fig. 5, *A* and *B*). To assure that PP19 inhibits clathrin-mediated endocytosis, we monitored endocytosis of Alexa568-labeled transferrin in THALs by fluorescence microscopy and found that PP19 blocked transferrin internalization by 36 ± 3% (*, $p < 0.05$). As expected, inhibition of dynamin with dynasore-blunted transferrin internalization by 43 ± 3% (*, $p < 0.05$) (Fig. 5*C*). We confirmed peptide transfection using a FITC-labeled PP19 peptide and examined THAL cells by fluorescence microscopy (Fig. 5*D*). Our data are consistent with partial inhibition of clathrin-mediated endocytosis by chlorpromazine and PP19 and indicate that this pathway is partly responsible for NKCC2 retrieval from the plasma membrane in the native renal epithelium.

Disruption of Lipid Rafts Blunts NKCC2 Endocytosis in THALs—We previously showed that NKCC2 endocytosis is completely blocked by depletion of cholesterol in the plasma membrane (16), and previous reports suggest that a fraction of NKCC2 partitions into lipid raft domains (50, 51). Therefore, a fraction of surface NKCC2 may be internalized by the lipid raft endocytic pathway. To test this, we studied the effect of disrupting lipid rafts with the cholesterol sequestering agent filipin III, on NKCC2 endocytosis. We found that filipin III at 2.5 μM blunted the rate of NKCC2 endocytosis by 39 ± 5% (Fig. 6, *A* and *B*) without affecting the total NKCC2 pool in THALs. Higher concentrations of filipin III were not used for these experiments because they decreased the total pool of NKCC2 by an unknown mechanism.

Caveolin-1 is one of the most abundant lipid raft proteins and is required for trafficking of lipid raft components to the plasma membrane, thus, depletion of caveolin-1 inhibits lipid raft-me-

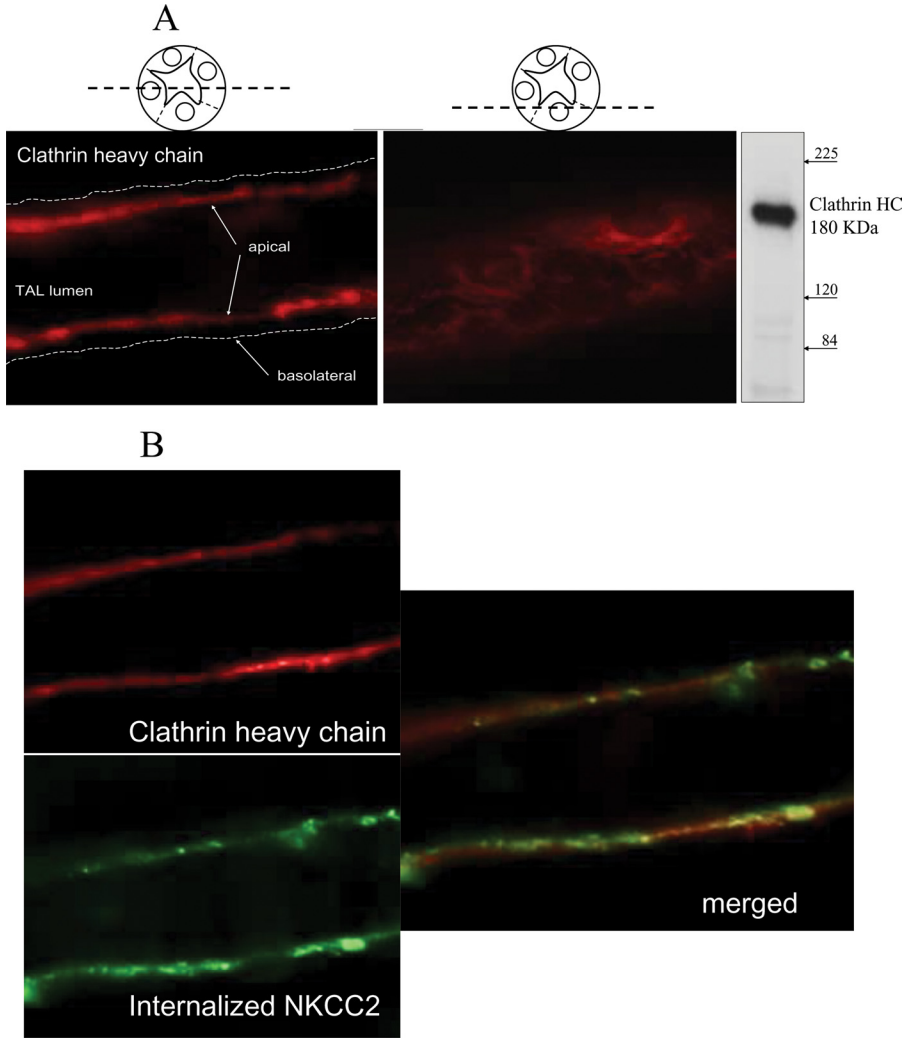

FIGURE 3. **Subapical localization of clathrin heavy chain and co-localization with internalized NKCC2 in THALs.** *A*, localization of clathrin heavy chain in the apical membrane and subapical space in isolated perfused THALs. THALs were isolated perfused and fixed and clathrin heavy chain immunolabeled as detailed under "Experimental Procedures." Inmunoblot shows a single band representing clathrin heavy chain at the expected molecular mass (~180 kDa). *B*, internalized NKCC2 is observed in subapical punctae and larger subapical structures also labeled for clathrin heavy chain in THALs. Apical surface NKCC2 was labeled with an exofacial antibody at 4 °C and allowed to internalize for 15 min (*green*). The label in surface NKCC2 was removed by acid-wash and THALs fixed and immunolabeled for clathrin heavy chain (*red*).

diated endocytosis (52). To disrupt lipid rafts in THALs, we decreased caveolin-1 expression *in vivo* by transduction of a shRNA against caveolin-1 (Ad-siRNACav-1) as described previously (40, 41). Ad-shRNACav-1 decreased caveolin-1 expression by 60% ($p < 0.01$) (Fig. 6*C*). Silencing caveolin-1 decreased the rate of NKCC2 endocytosis by 30 ± 4% (Fig. 6, *D* and *E*). These data suggest that disruption of lipid rafts by decreasing caveolin-1 inhibits NKCC2 endocytosis.

Because our data showed that NKCC2 endocytosis is mediated by both clathrin- and lipid raft-dependent pathways, we studied whether blocking the two pathways simultaneously would further inhibit NKCC2 endocytosis. We found that treating THALs with chlorpromazine and filipin III inhibited the rate of NKCC2 endocytosis by 69 ± 11% (Fig. 7, *A* and *B*) without affecting the total pool of NKCC2. Although the combination of Chlorpromazine and Filipin III was additive, it did not completely eliminate NKCC2 endocytosis. To determine whether these pathways mediate all NKCC2 endocytosis, we used a novel small molecule inhibitor of clathrin-mediated endocytosis (Pitstop2, IC_{50}: 12 μM) (53) in combination with the cholesterol-depleting agent MβCD, which blocks lipid raft dependent endocytosis (33, 54–58). We found that treating THALs with Pitstop alone (30 μM) inhibited NKCC2 endocytosis at 15 min by 40% ($p < 0.05$). Inhibiting clathrin- and lipid raft-mediated endocytosis simultaneously, completely blocked endocytosis ($p < 0.05$ *versus* Pitstop2 alone), such that the signal obtained was not significantly different from cero (Baseline: 18.8 ± 2.9%; Pitstop2: 11.6 ± 1.2; Pitstop2 + MbCD 5 mM: 2.4 ± 0.5%; $n = 5$; $p < 0.05$)(Fig. 8*A* and *B*). The total pool of NKCC2 was not affected by the treatment. These data indicate that both pathways mediate NKCC2 endocytosis.

DISCUSSION

We previously reported that NKCC2-dependent NaCl transport is modulated by changes in steady-state surface NKCC2 levels in the THAL (15, 17). NKCC2 undergoes constitutive exocytic trafficking which is stimulated by the cAMP signaling pathway (18). To maintain steady-state surface levels, NKCC2

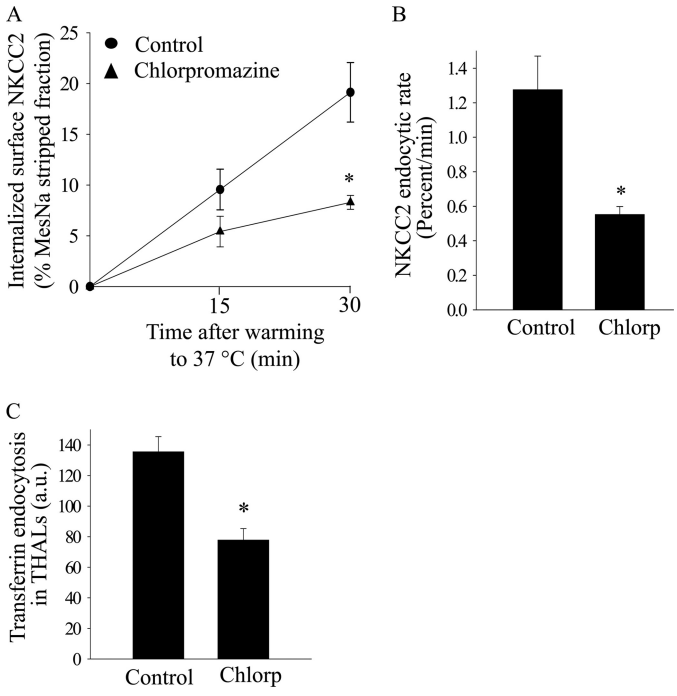

FIGURE 4. **Effect of clathrin inhibition with chlorpromazine on NKCC2 retrieval in THALs.** *A*, cumulative data showing the effect of chlorpromazine (20 μM) on constitutive NKCC2 endocytosis in THALs. THAL suspensions were incubated at 37 °C for 15 and 30 min in the absence (control, *circles*) or presence of chlorpromazine (20 μM) (*triangles*). Endocytosed NKCC2 was detected by Western blot as described in "Experimental Procedures" and mean optical density quantified by densitometry. Basal: 15 min, 9.6 ± 2.0%; 30 min, 19.1 ± 2.9%; chlorpromazine: 15 min, 5.4 ± 1.5%; 30 min, 8.3 ± 0.7%; $n = 4$, *, $p < 0.05$). Data are expressed as a percentage of the MesNa-stripped fraction. *B*, quantification of NKCC2 trafficking rate, derived from the slopes of the data shown in *A*. Basal: 1.27 ± 0.19% per min; chlorpromazine: 0.55 ± 0.04% per min; $n = 4$; *, $p < 0.05$. *C*, cumulative data for constitutive transferrin endocytosis. THALs were equilibrated with vehicle or chlorpromazine for 15 min at 37 °C and then transferrin was added to the bath for 30 min. Basal, 135.5 ± 9.8 a.u.; chlorpromazine (20 μM): 77.8 ± 7.5 a.u. (from 5 preparations, 65 and 63 tubules, respectively; *, $p < 0.05$).

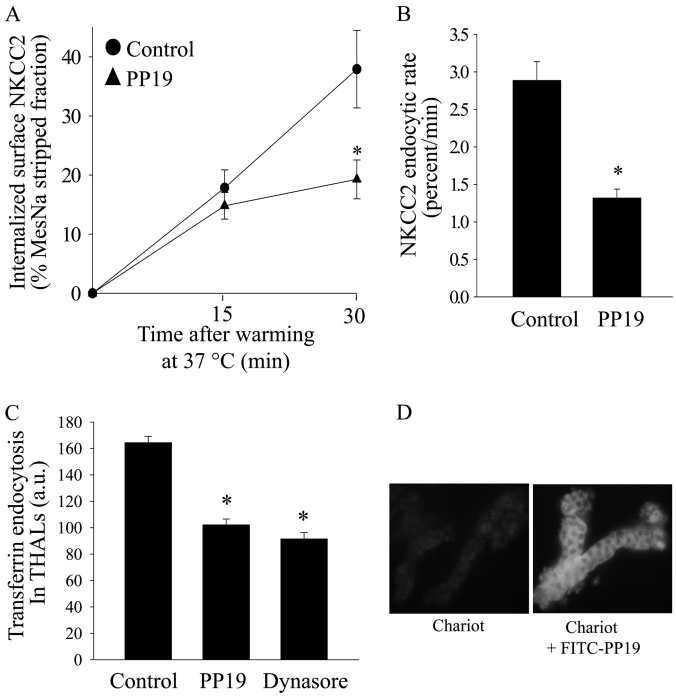

FIGURE 5. **Effect of clathrin inhibition by transduction of PP19 on NKCC2 retrieval in THALs.** *A*, cumulative data showing the effect of the PP19 peptide (6 μM) on constitutive NKCC2 endocytosis in THALs. THAL suspensions were incubated at 37 °C for 15 and 30 min in the presence of vehicle (Chariot carrier, *circles*) or carrier plus PP19 (6 μM) (*triangles*). Endocytosed NKCC2 was detected by Western blot as described in "Experimental Procedures" and mean optical density quantified by densitometry. Basal: 15 min, 17.8 ± 3.2%; 30 min, 37.9 ± 6.6%; PP19: 15 min, 14.8 ± 2.9%; 30 min, 19.3 ± 3.3%; $n = 6$, *, $p < 0.05$. Data are expressed as a percentage of the MesNa-stripped fraction. Error bars represent S.E. *B*, quantification of NKCC2 trafficking rate derived from the slopes of the data shown in *A*. Basal: 2.88 ± 0.25% per min; PP19: 1.32 ± 0.11% per min ($n = 6$, *, $p < 0.05$). *Error bars* represent S.E. *C*, cumulative data for constitutive transferrin endocytosis. THALs were incubated for 30 min with Chariot, then aliquoted and equilibrated for 15 min at 37 °C with vehicle, PP19 or 100 μM dynasore, and transferrin was added to the bath for 30 min. Vehicle = 164.4 ± 4.7 a.u.; PP19 (6 μM): 102.1 ± 4.4 a.u.; dynasore (100 μM): 91.5 ± 4.7 a.u.; (from 5 preparations, 74, 68, and 60 tubules, respectively; *, $p < 0.05$). *D*, representative images of THALs incubated with Chariot in the absence or presence of PP19-FITC. THAL suspensions were preincubated with Chariot, then incubated at 37 °C for 30 min in the absence or presence of PP19-FITC (6 μM). *Green* indicates positive PP19-FITC fluorescence (magnification ×40). Tubules treated with Chariot in the absence of PP19 did not exhibit significantly different fluorescence from background.

undergoes endocytosis in a cholesterol-dependent manner and a large fraction of the internalized pool is recycled back to the plasma membrane (16). Thus the endocytic pathway determines steady-state surface NKCC2 levels as well as the size of the recycling pool. However, the pathway and proteins involved in NKCC2 endocytosis are unknown. We observed that inhibition of dynamin-2, clathrin, and lipid raft-dependent endocytosis blunted the rate of NKCC2 endocytosis and increased steady-state surface NKCC2 levels. Our data indicate that dynamin-2, clathrin and lipid rafts-dependent endocytosis, mediate constitutive NKCC2 endocytosis in THALs.

Our earlier data and those of others suggest that trafficking of NKCC2 is critical for maintaining steady-state surface NKCC2 levels in the plasma membrane as well as the capacity of the THAL to reabsorb NaCl (15–18, 59). However, the proteins involved in dynamic NKCC2 trafficking into and out of the apical membrane have not been identified to our knowledge. Membrane proteins can be endocytosed by a variety of pathways, including clathrin- or lipid raft/caveolin1-mediated endocytosis, macropinocytosis, and clathrin- and caveolae-independent endocytosis (60–63). To study the role of dynamin, we used dynasore, which is a potent inhibitor of dynamin activity (47, 48) and expression of dominant negative dynamin2 (K44A) (25, 64, 65). Dynamin inhibition blocked the rate of NKCC2 endocytosis by ~56% and increased steady-state surface NKCC2 levels by ~60%. Expression of the dominant negative Dyn2(K44A) in THALs blocked the rate of NKCC2 endocytosis by ~38% and increased steady-state surface NKCC2 levels by ~38%. While it is not clear why dynasore inhibited NKCC2 endocytosis to a greater extent than Dyn2(K44A), this could be due to the fact that it takes at least 6 to 7 days for Dyn2(K44A) to reach maximal expression and inhibit endocytosis (40, 41), allowing sufficient time for compensatory retrieval mechanisms to develop. It is also possible that Dyn2(K44A) exerts competitive inhibition on dynamin-2, whereas dynasore acutely inhibits endocytosis by non-competitive inhibition (47, 48). In addition, expression levels of the dynamin-2 mutant *in vivo* may not be high enough to block all endogenous dynamin-2 activity. To our knowledge, expression of dynamin-1 or dynamin-3 has not been demonstrated in the

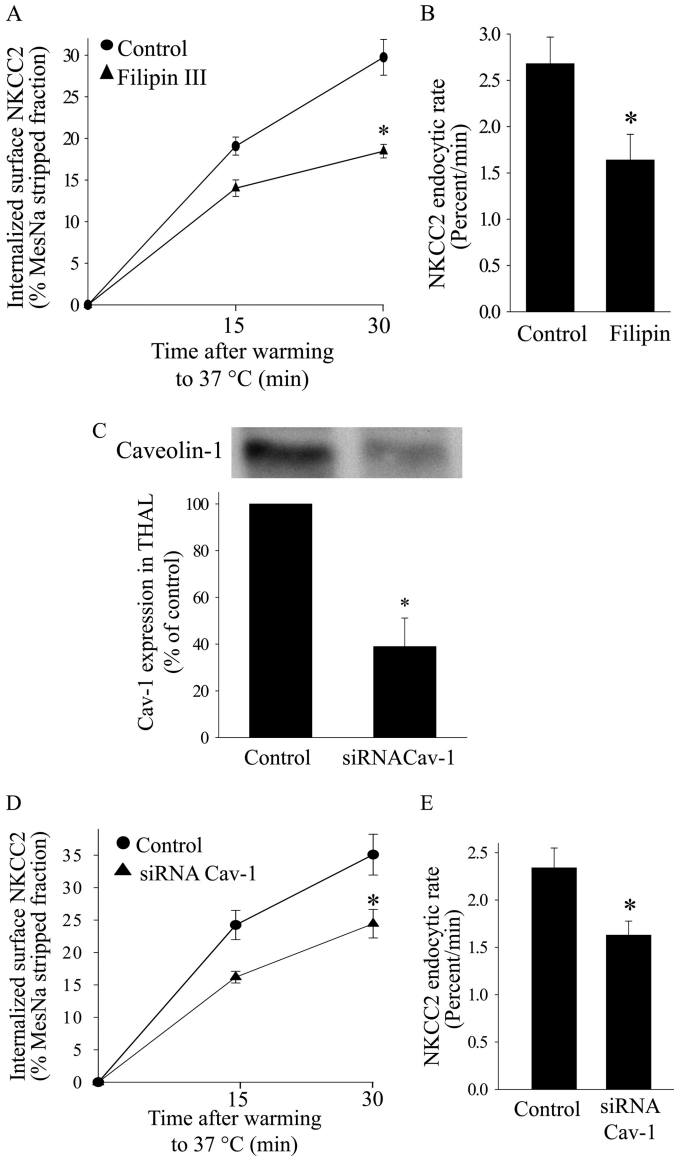

FIGURE 6. **Effect of lipid raft disruption on NKCC2 retrieval in THALs.** *A*, cumulative data showing the effect of filipin III (2.5 μM) on constitutive NKCC2 endocytosis in THALs. Control or THALs treated with filipin III (2.5 μM) were biotinylated and incubated at 37 °C for 15 or 30 min (Basal 15 min, 19.1 ± 1.1%; 30 min, 29.8 ± 2.1%; siRNACav1 15 min, 14.0 ± 1.0%; 30 min, 17.9 ± 0.8%; $n = 5$, *, $p < 0.05$). Data are expressed as a percentage of the MesNa-stripped fraction. *B*, quantification of NKCC2 trafficking rate derived from the slopes of the data shown in *A*. Basal: 2.68 ± 0.28% per min; filipin: 1.64 ± 0.27% per min ($n = 5$, *, $p < 0.05$). Error bars represent S.E. *C*, representative Western blot showing the effect of siRNACav1 on caveolin-1 expression in rat medullary THALs. Control: 100%; siRNACav1: 39 ± 12%; $n = 3$; *, $p < 0.05$. *D*, cumulative data for constitutive NKCC2 endocytosis over time in THAL suspensions under basal conditions (*full line*) or after transduction with Ad-siRNACav1 (*dotted line*). *In vivo* adenovirus-mediated gene transfer of siRNACav1 was performed as described in "Experimental Procedures." THALs from control or siRNACav1-transduced kidneys were biotinylated and incubated at 37 °C for 15 or 30 min (Basal 15 min, 24.2 ± 2.3%; 30 min, 35.1 ± 3.2%; siRNACav1 15 min, 16.2 ± 0.9%; 30 min, 24.4 ± 2.2%: $n = 7$, *, $p < 0.05$). Data are expressed as a percentage of the MesNa-stripped fraction. *E*, quantification of NKCC2 trafficking rate derived from the slopes of the data shown in A. Basal: 2.34 ± 0.21% per min; siRNACav1: 1.63 ± 0.15% per min; $n = 7$, *, $p < 0.05$. *Error bars* represent S.E.

renal epithelium (66, 67) suggesting a predominant role of dynamin-2 in trafficking by renal epithelial transporters like NKCC2.

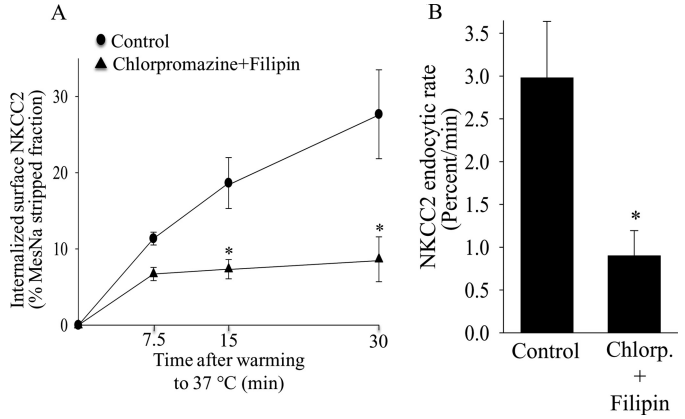

FIGURE 7. **Effect of clathrin inhibition and lipid raft disruption on NKCC2 retrieval in THALs.** *A*, cumulative data showing the effect of simultaneous treatment with the clathrin inhibitor chlorpromazine (20 μM) and lipid-raft disrupting agent filipin III (2.5 μM) on NKCC2 endocytosis in THALs. Basal: 15 min, 18.6 ± 3.3%; 30 min, 27.7 ± 8.8%; chlorpromazine + filipin: 15 min, 7.3 ± 1.1%; 30 min, 8.6 ± 2.8%; $n = 6$, *, $p < 0.05$. Data are expressed as a percentage of the MesNa-stripped fraction. Error bars represent S.E. *B*, quantification of NKCC2 trafficking rate derived from the slopes of the data shown in *A*. Basal: 2.98 ± 0.54% per min; chlorpromazine + filipin: 0.99 ± 0.25% per min; $n = 6$, *, $p < 0.05$. *Error bars* represent S.E.

Regulation of dynamin-2-mediated endocytosis in epithelial cells is poorly understood. Endocytosis requires coordinated steps involving several proteins, and most cell culture data suggest that phosphorylation and protein-protein interactions are important for regulation of dynamin-2 activity. Some of the proteins known to be associated with dynamin-2 are sorting nexin 9 (SNX9), adaptor protein 2 (AP2), clathrin, and aldolase B (68). SNX9 binds the proline rich domain of dynamin-2 in an ATP-dependent manner (69). Aldolase B binds to SNX9 with high affinity, thereby decreasing its membrane binding activity and inhibiting endocytosis. However, phosphorylation of SNX9 releases aldolase B from this complex, allowing SNX9-Dyn2 complex formation. Aldolase B is one of the few proteins known to interact with NKCC2; however, in a cell culture system, expression of aldolase B was found to decrease steady-state surface NKCC2 levels and activity (59). While endocytosis of NKCC2 was not measured in that study it is possible that the aldolase B-SNX9 complex plays a role in regulating dynamin-2 mediated NKCC2 internalization. We know of no report showing whether physiological agonists or hormones stimulate or inhibit dynamin-2 activity in epithelial cells. Given the important role of dynamin-2 in NKCC2 trafficking, its regulatory processes would seem to call for further study.

We previously showed that cholesterol depletion with MβCD blocked NKCC2 endocytosis by 90% (16). However, MβCD inhibits clathrin as well as lipid raft-dependent/caveolin-1 endocytic pathways (57, 58, 70). Most apical renal Na^+ transporters are internalized via a clathrin-mediated pathway (25, 27, 31, 33), whereas there is little evidence regarding the role of caveolin-1 in apical endocytosis. Thus, we focused on the clathrin-mediated endocytic pathway. Chlorpromazine, which has been used extensively to inhibit clathrin-mediated endocytosis (28, 71), blunted the rate of NKCC2 endocytosis by ~52%. In addition transducing THALs with a peptide (PP19) that inhibits the protein complex between clathrin, endophilin, and synaptojanin (44) blunted the rate of NKCC2 endocytosis by

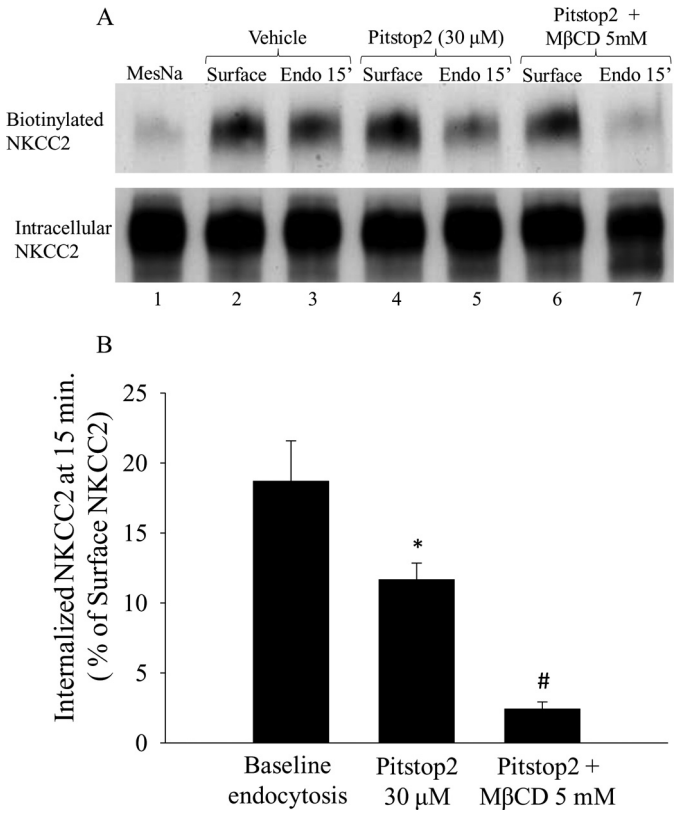

FIGURE 8. **Additive effect of clathrin- and lipid-raft mediated endocytosis inhibitors on NKCC2 retrieval in THALs.** *A*, representative Western blot showing surface NKCC2 and internalized NKCC2 at 15 min in biotinylated THALs treated with: MesNa (*lane 1*), vehicle (DMSO) (*lanes 2*, *3*), clathrin inhibitor (Pitstop2, 30 μM) (*lanes 4*, *5*), and clathrin inhibitor (Pitstop2) plus the cholesterol-chelating agent MβCD, 5 mM (*lanes 6* and *7*). *B*, cumulative data showing the effect of simultaneous treatment with the clathrin inhibitor Pitstop2 (30 μM) and methyl-β-cyclodextrin (5 mM) on NKCC2 endocytosis at 15 min. Baseline: 18.8 $\pm$ 2.9%; Pitstop2: 11.6 $\pm$ 1.2; Pitstop2 + MβCD (5 mM): 2.5 $\pm$ 0.5%; $n = 5$. *, $p < 0.05$ *versus* baseline, and #, $p < 0.05$ compared with Pitstop2. Data are expressed as a percentage of the MesNa-stripped surface NKCC2 fraction. *Error bars* represent S.E.

~52%. Taken together, these data indicate that NKCC2 undergoes constitutive endocytosis in part via a clathrin-mediated pathway.

Stimulation of NKCC2 recycling by the inhibitors used may have influenced the results we obtained when measuring internalization of biotinylated NKCC2. We found that both dynasore and chlorpromazine decreased the rate of NKCC2 recycling. This effect does not invalidate our conclusion but rather strengthens it, because the net result is underestimation of the NKCC2 endocytosis inhibition by these drugs. Others have shown that chlorpromazine inhibits recycling (72).

Biochemical studies indicate that a fraction of NKCC2 partitions into Triton X-100 insoluble lipid raft fractions (50, 51). We found that filipin III, a lipid raft-disrupting agent, decreased the rate of NKCC2 endocytosis by ~30%, suggesting that endocytosis of NKCC2 is mediated in part via a lipid raft-dependent mechanism. We know of no quantitative data addressing which fraction of surface NKCC2 is located in lipid rafts. Differential plasma membrane distribution has been observed for others renal transporters located in lipid rafts (75–78), although this does not apply to all membrane proteins (79). In the case of NHE3, ~20% of the surface pool seems to be located in lipid rafts, and this fraction is sensitive to epidermal growth factor-dependent regulation (80).

Caveolin-1 has been used to identify and study the lipid raft compartment (73). Endocytosis via the lipid raft-mediated pathway is inhibited by decreasing caveolin-1 expression (74). We found that decreasing caveolin-1 expression by ~60% blunted NKCC2 endocytosis by 30%. A similar effect has been observed for other membrane proteins in different cells (74). Taken together, our data indicate that NKCC2 endocytosis occurs at least in part via clathrin- and lipid raft-dependent pathways. To study if all NKCC2 endocytosis was mediated by these two pathways we tested whether inhibiting both pathways would completely block constitutive NKCC2 internalization. Inhibition of clathrin-mediated endocytosis with Pitstop2 (53), (a novel small molecule inhibitor) partially blocked constitutive NKCC2 internalization, which was completely blocked when combined with a cholesterol-depleting dextrin (MβCD), an agent that blocks both clathrin- and lipid raft-mediated endocytosis. The combined inhibition of lipid raft- and clathrin-mediated endocytosis was complete and significantly greater than clathrin inhibition alone. These data suggest that clathrin- and cholesterol-sensitive lipid rafts pathways mediate all of the constitutive NKCC2 endocytosis in native THALs.

Overall, we believe our data provide the first evidence that NKCC2 endocytosis is mediated in part via dynamin-2, clathrin- and lipid raft-dependent pathways in renal epithelium. We conclude that NKCC2 undergoes constitutive endocytosis in native THALs primarily via a dynamin-2 mediated pathway. In addition, both clathrin- and lipid raft-mediated pathways contribute to apical internalization of the cotransporter. This trafficking process is important for maintenance of steady-state surface NKCC2 levels and overall regulation of NaCl transport by the kidney.

Acknowledgments—We thank Elizabeth Furest for thorough reading of the manuscript and secretarial assistance. We thank Dr. Mark McNiven for generously providing the rat dynamin-2 with a single point mutation of lysine 44 to alanine (dyn2K44A) and Dr. Debbie C. Thurmond for generously supplying the Ad-shRNA-Cav1.

REFERENCES

1. Russell, J. M. (2000) Sodium-potassium-chloride cotransport. *Physiol. Rev.* **80,** 211–276
2. Gamba, G. (2005) Molecular physiology and pathophysiology of electroneutral cation-chloride cotransporters. *Physiol. Rev.* **85,** 423–493
3. Nielsen, S., Maunsbach, A. B., Ecelbarger, C. A., and Knepper, M. A. (1998) Ultrastructural localization of Na-K-2Cl cotransporter in thick ascending limb and macula densa of rat kidney. *Am. J. Physiol.* **275,** F885-F893
4. Ecelbarger, C. A., Terris, J., Hoyer, J. R., Nielsen, S., Wade, J. B., and Knepper, M. A. (1996) Localization and regulation of the rat renal Na(+)-K(+)-2Cl- cotransporter, BSC-1. *Am. J. Physiol.* **271,** F619-F628
5. Obermüller, N., Kunchaparty, S., Ellison, D. H., and Bachmann, S. (1996) Expression of the Na-K-2Cl cotransporter by macula densa and thick ascending limb cells of rat and rabbit nephron. *J. Clin. Invest.* **98,** 635–640
6. Pressler, C. A., Heinzinger, J., Jeck, N., Waldegger, P., Pechmann, U., Reinalter, S., Konrad, M., Beetz, R., Seyberth, H. W., and Waldegger, S. (2006) Late-onset manifestation of antenatal Bartter syndrome as a result of residual function of the mutated renal Na+-K+-2Cl- co-transporter. *J. Am. Soc. Nephrol.* **17,** 2136–2142

7. Starremans, P. G., Kersten, F. F., Knoers, N. V., van den Heuvel, L. P., and Bindels, R. J. (2003) Mutations in the human Na-K-2Cl cotransporter (NKCC2) identified in Bartter syndrome type I consistently result in non-functional transporters. *J. Am. Soc. Nephrol.* **14,** 1419–1426
8. Hoagland, K. M., Flasch, A. K., Dahly-Vernon, A. J., dos Santos, E. A., Knepper, M. A., and Roman, R. J. (2004) Elevated BSC-1 and ROMK expression in Dahl salt-sensitive rat kidneys. *Hypertension* **43,** 860–865
9. Sonalker, P. A., Tofovic, S. P., and Jackson, E. K. (2004) Increased expression of the sodium transporter BSC-1 in spontaneously hypertensive rats. *J. Pharmacol. Exp. Ther.* **311,** 1052–1061
10. Kirchner, K. A. (1992) Increased loop chloride uptake precedes hypertension in Dahl salt-sensitive rats. *Am. J. Physiol.* **262,** R263–R268
11. Kirchner, K. A. (1990) Greater loop chloride uptake contributes to blunted pressure natriuresis in Dahl salt sensitive rats. *J. Am. Soc. Nephrol.* **1,** 180–186
12. Aviv, A., Hollenberg, N. K., and Weder, A. (2004) Urinary potassium excretion and sodium sensitivity in blacks. *Hypertension* **43,** 707–713
13. Chun, T. Y., Bankir, L., Eckert, G. J., Bichet, D. G., Saha, C., Zaidi, S. A., Wagner, M. A., and Pratt, J. H. (2008) Ethnic differences in renal responses to furosemide. *Hypertension* **52,** 241–248
14. Weder, A. B., Gleiberman, L., and Sachdeva, A. (2009) Whites excrete a water load more rapidly than blacks. *Hypertension* **53,** 715–718
15. Ares, G. R., Caceres, P., Alvarez-Leefmans, F. J., and Ortiz, P. A. (2008) cGMP decreases surface NKCC2 levels in the thick ascending limb: role of phosphodiesterase 2 (PDE2). *Am. J. Physiol. Renal Physiol.* **295,** F877–F887
16. Ares, G. R., and Ortiz, P. A. (2010) Constitutive endocytosis and recycling of NKCC2 in rat thick ascending limbs. *Am. J. Physiol. Renal Physiol.* **299,** F1193–F1202
17. Ortiz, P. A. (2006) cAMP increases surface expression of NKCC2 in rat thick ascending limbs: role of VAMP. *Am. J. Physiol. Renal Physiol.* **290,** F608–F616
18. Caceres, P. S., Ares, G. R., and Ortiz, P. A. (2009) cAMP stimulates apical exocytosis of the renal Na(+)-K(+)-2Cl(-) cotransporter NKCC2 in the thick ascending limb: role of protein kinase A. *J. Biol. Chem.* **284,** 24965–24971
19. Hinshaw, J. E. (2000) Dynamin and its role in membrane fission. *Annu. Rev. Cell Dev. Biol.* **16,** 483–519
20. McNiven, M. A., Cao, H., Pitts, K. R., and Yoon, Y. (2000) *Trends Biochem. Sci.* **25,** 115–120
21. Henley, J. R., Krueger, E. W., Oswald, B. J., and McNiven, M. A. (1998) Dynamin-mediated internalization of caveolae. *J. Cell Biol.* **141,** 85–99
22. Cao, H., Chen, J., Awoniyi, M., Henley, J. R., and McNiven, M. A. (2007) Dynamin 2 mediates fluid-phase micropinocytosis in epithelial cells. *J. Cell Sci.* **120,** 4167–4177
23. Cook, T. A., Urrutia, R., and McNiven, M. A. (1994) Identification of dynamin 2, an isoform ubiquitously expressed in rat tissues. *Proc. Natl. Acad. Sci. U.S.A.* **91,** 644–648
24. Collazo, R., Fan, L., Hu, M. C., Zhao, H., Wiederkehr, M. R., and Moe, O. W. (2000) Acute regulation of Na+/H+ exchanger NHE3 by parathyroid hormone via NHE3 phosphorylation and dynamin-dependent endocytosis. *J. Biol. Chem.* **275,** 31601–31608
25. Shimkets, R. A., Lifton, R. P., and Canessa, C. M. (1997) The activity of the epithelial sodium channel is regulated by clathrin-mediated endocytosis. *J. Biol. Chem.* **272,** 25537–25541
26. Karpushev, A. V., Levchenko, V., Pavlov, T. S., Lam, V. Y., Vinnakota, K. C., Vandewalle, A., Wakatsuki, T., and Staruschenko, A. (2008) Regulation of ENaC expression at the cell surface by Rab11. *Biochem. Biophys. Res. Commun.* **377,** 521–525
27. Sun, T. X., Van Hoek, A., Huang, Y., Bouley, R., McLaughlin, M., and Brown, D. (2002) Aquaporin-2 localization in clathrin-coated pits: inhibition of endocytosis by dominant-negative dynamin. *Am. J. Physiol. Renal Physiol.* **282,** F998–F1011
28. Puri, V., Watanabe, R., Singh, R. D., Dominguez, M., Brown, J. C., Wheatley, C. L., Marks, D. L., and Pagano, R. E. (2001) Clathrin-dependent and -independent internalization of plasma membrane sphingolipids initiates two Golgi targeting pathways. *J. Cell Biol.* **154,** 535–547
29. Howes, M. T., Kirkham, M., Riches, J., Cortese, K., Walser, P. J., Simpson, F., Hill, M. M., Jones, A., Lundmark, R., Lindsay, M. R., Hernandez-Deviez, D. J., Hadzic, G., McCluskey, A., Bashir, R., Liu, L., Pilch, P., McMahon, H., Robinson, P. J., Hancock, J. F., Mayor, S., and Parton, R. G. (2010) Clathrin-independent carriers form a high capacity endocytic sorting system at the leading edge of migrating cells. *J. Cell Biol.* **190,** 675–691
30. Owen, D. J., Collins, B. M., and Evans, P. R. (2004) Adaptors for clathrin coats: structure and function. *Annu. Rev. Cell Dev. Biol.* **20,** 153–191
31. Chow, C. W., Khurana, S., Woodside, M., Grinstein, S., and Orlowski, J. (1999) The epithelial Na(+)/H(+) exchanger, NHE3, is internalized through a clathrin-mediated pathway. *J. Biol. Chem.* **274,** 37551–37558
32. Lukacs, G. L., Segal, G., Kartner, N., Grinstein, S., and Zhang, F. (1997) Constitutive internalization of cystic fibrosis transmembrane conductance regulator occurs via clathrin-dependent endocytosis and is regulated by protein phosphorylation. *Biochem. J.* **328,** 353–361
33. Huang, H., Feng, X., Zhuang, J., Fröhlich, O., Klein, J. D., Cai, H., Sands, J. M., and Chen, G. (2010) Internalization of UT-A1 urea transporter is dynamin dependent and mediated by both caveolae- and clathrin-coated pit pathways. *Am. J. Physiol. Renal Physiol.* **299,** F1389–F1395
34. Welker, P., Böhlick, A., Mutig, K., Salanova, M., Kahl, T., Schlüter, H., Blottner, D., Ponce-Coria, J., Gamba, G., and Bachmann, S. (2008) Renal Na+-K+-Cl- cotransporter activity and vasopressin-induced trafficking are lipid raft-dependent. *Am. J. Physiol. Renal Physiol.* **295,** F789-F802
35. Yu, M. J., Pisitkun, T., Wang, G., Aranda, J. F., Gonzales, P. A., Tchapyjnikov, D., Shen, R. F., Alonso, M. A., and Knepper, M. A. (2008) Large-scale quantitative LC-MS/MS analysis of detergent-resistant membrane proteins from rat renal collecting duct. *Am. J. Physiol. Cell Physiol.* **295,** C661–C678
36. Orth, J. D., Krueger, E. W., Cao, H., and McNiven, M. A. (2002) The large GTPase dynamin regulates actin comet formation and movement in living cells. *Proc. Natl. Acad. Sci. U.S.A.* **99,** 167–172
37. Weller, S. G., Capitani, M., Cao, H., Micaroni, M., Luini, A., Sallese, M., and McNiven, M. A. (2010) Src kinase regulates the integrity and function of the Golgi apparatus via activation of dynamin 2. *Proc. Natl. Acad. Sci. U.S.A.* **107,** 5863–5868
38. Nevins, A. K., and Thurmond, D. C. (2006) Caveolin-1 functions as a novel Cdc42 guanine nucleotide dissociation inhibitor in pancreatic beta-cells. *J. Biol. Chem.* **281,** 18961–18972
39. Cao, H., Chen, J., Krueger, E. W., and McNiven, M. A. (2010) SRC-mediated phosphorylation of dynamin and cortactin regulates the "constitutive" endocytosis of transferrin. *Mol. Cell Biol.* **30,** 781–792
40. Ortiz, P. A., Hong, N. J., Wang, D., and Garvin, J. L. (2003) Gene transfer of eNOS to the thick ascending limb of eNOS-KO mice restores the effects of L-arginine on NaCl absorption. *Hypertension* **42,** 674–679
41. Ortiz, P. A., Hong, N. J., Plato, C. F., Varela, M., and Garvin, J. L. (2003) An *in vivo* method for adenovirus-mediated transduction of thick ascending limbs. *Kidney Int.* **63,** 1141–1149
42. Damke, H., Baba, T., Warnock, D. E., and Schmid, S. L. (1994) Induction of mutant dynamin specifically blocks endocytic coated vesicle formation. *J. Cell Biol.* **127,** 915–934
43. Maxfield, F. R., and McGraw, T. E. (2004) Endocytic recycling. *Nat. Rev. Mol. Cell Biol.* **5,** 121–132
44. Gad, H., Ringstad, N., Löw, P., Kjaerulff, O., Gustafsson, J., Wenk, M., Di Paolo, G., Nemoto, Y., Crun, J., Ellisman, M. H., De Camilli, P., Shupliakov, O., and Brodin, L. (2000) Fission and uncoating of synaptic clathrin-coated vesicles are perturbed by disruption of interactions with the SH3 domain of endophilin. *Neuron* **27,** 301–312
45. Chan, S. A., and Smith, C. (2003) Low frequency stimulation of mouse adrenal slices reveals a clathrin-independent, protein kinase C-mediated endocytic mechanism. *J. Physiol.* **553,** 707–717
46. Fulop, T., Doreian, B., and Smith, C. (2008) Dynamin I plays dual roles in the activity-dependent shift in exocytic mode in mouse adrenal chromaffin cells. *Arch. Biochem. Biophys.* **477,** 146–154
47. Newton, A. J., Kirchhausen, T., and Murthy, V. N. (2006) Inhibition of dynamin completely blocks compensatory synaptic vesicle endocytosis. *Proc. Natl. Acad. Sci. U.S.A.* **103,** 17955–17960
48. Macia, E., Ehrlich, M., Massol, R., Boucrot, E., Brunner, C., and Kirchhausen, T. (2006) Dynasore, a cell-permeable inhibitor of dynamin. *Dev. Cell* **10,** 839–850

49. Schmid, S. L. (1997) Clathrin-coated vesicle formation and protein sorting: an integrated process. *Annu. Rev. Biochem.* **66,** 511–548
50. Welker, P., Böhlick, A., Mutig, K., Salanova, M., Kahl, T., Schlüter, H., Blottner, D., Ponce-Coria, J., Gamba, G., and Bachmann, S. (2008) Renal Na+-K+-Cl- cotransporter activity and vasopressin-induced trafficking are lipid raft-dependent. *Am. J. Physiol. Renal Physiol.* **295,** F789–F802
51. Yu, M. J., Pisitkun, T., Wang, G., Aranda, J. F., Gonzales, P. A., Tchapyjnikov, D., Shen, R. F., Alonso, M. A., and Knepper, M. A. (2008) Large-scale quantitative LC-MS/MS analysis of detergent-resistant membrane proteins from rat renal collecting duct. *Am. J. Physiol. Cell Physiol.* **295,** C661–C678
52. Rajendran, L., and Simons, K. (2005) Lipid rafts and membrane dynamics. *J. Cell Sci.* **118,** 1099–1102
53. von Kleist, L., Stahlschmidt, W., Bulut, H., Gromova, K., Puchkov, D., Robertson, M. J., MacGregor, K. A., Tomilin, N., Pechstein, A., Chau, N., Chircop, M., Sakoff, J., von Kries, J. P., Saenger, W., Kräusslich, H. G., Shupliakov, O., Robinson, P. J., McCluskey, A., and Haucke, V. (2011) Role of the clathrin terminal domain in regulating coated pit dynamics revealed by small molecule inhibition. *Cell* **146,** 471–484
54. Chen, J., Chen, L., Wang, G., and Tang, H. (2007) Cholesterol-dependent and -independent CD40 internalization and signaling activation in cardiovascular endothelial cells. *Arterioscler. Thromb. Vasc. Biol.* **27,** 2005–2013
55. Le, P. U., Guay, G., Altschuler, Y., and Nabi, I. R. (2002) Caveolin-1 is a negative regulator of caveolae-mediated endocytosis to the endoplasmic reticulum. *J. Biol. Chem.* **277,** 3371–3379
56. Parpal, S., Karlsson, M., Thorn, H., and Strålfors, P. (2001) Cholesterol depletion disrupts caveolae and insulin receptor signaling for metabolic control via insulin receptor substrate-1, but not for mitogen-activated protein kinase control. *J. Biol. Chem.* **276,** 9670–9678
57. Rodal, S. K., Skretting, G., Garred, O., Vilhardt, F., van Deurs, B., and Sandvig, K. (1999) Extraction of cholesterol with methyl-beta-cyclodextrin perturbs formation of clathrin-coated endocytic vesicles. *Mol. Biol. Cell* **10,** 961–974
58. Subtil, A., Gaidarov, I., Kobylarz, K., Lampson, M. A., Keen, J. H., and McGraw, T. E. (1999) Acute cholesterol depletion inhibits clathrin-coated pit budding. *Proc. Natl. Acad. Sci. U.S.A.* **96,** 6775–6780
59. Benziane, B., Demaretz, S., Defontaine, N., Zaarour, N., Cheval, L., Bourgeois, S., Klein, C., Froissart, M., Blanchard, A., Paillard, M., Gamba, G., Houillier, P., and Laghmani, K. (2007) NKCC2 surface expression in mammalian cells: down-regulation by novel interaction with aldolase B. *J. Biol. Chem.* **282,** 33817–33830
60. Mayor, S., and Pagano, R. E. (2007) Pathways of clathrin-independent endocytosis. *Nat. Rev. Mol. Cell Biol.* **8,** 603–612
61. Traub, L. M. (2009) Tickets to ride: selecting cargo for clathrin-regulated internalization. *Nat. Rev. Mol. Cell Biol.* **10,** 583–596
62. Gundelfinger, E. D., Kessels, M. M., and Qualmann, B. (2003) Temporal and spatial coordination of exocytosis and endocytosis. *Nat. Rev. Mol. Cell Biol.* **4,** 127–139
63. Sorkin, A., and von Zastrow, M. (2009) Endocytosis and signaling: intertwining molecular networks. *Nat. Rev. Mol. Cell Biol.* **10,** 609–622
64. Hryciw, D. H., Ekberg, J., Lee, A., Lensink, I. L., Kumar, S., Guggino, W. B., Cook, D. I., Pollock, C. A., and Poronnik, P. (2004) Nedd4–2 functionally interacts with ClC-5: involvement in constitutive albumin endocytosis in proximal tubule cells. *J. Biol. Chem.* **279,** 54996–55007
65. Subramanya, A. R., Liu, J., Ellison, D. H., Wade, J. B., and Welling, P. A. (2009) WNK4 diverts the thiazide-sensitive NaCl cotransporter to the lysosome and stimulates AP-3 interaction. *J. Biol. Chem.* **284,** 18471–18480
66. Okamoto, P. M., Herskovits, J. S., and Vallee, R. B. (1997) Role of the basic, proline-rich region of dynamin in Src homology 3 domain binding and endocytosis. *J. Biol. Chem.* **272,** 11629–11635
67. Cao, H., Garcia, F., and McNiven, M. A. (1998) Differential distribution of dynamin isoforms in mammalian cells. *Mol. Biol. Cell* **9,** 2595–2609
68. Rangarajan, E. S., Park, H., Fortin, E., Sygusch, J., and Izard, T. (2010) Mechanism of aldolase control of sorting nexin 9 function in endocytosis. *J. Biol. Chem.* **285,** 11983–11990
69. Lundmark, R., and Carlsson, S. R. (2004) Regulated membrane recruitment of dynamin-2 mediated by sorting nexin 9. *J. Biol. Chem.* **279,** 42694–42702
70. Klein, U., Gimpl, G., and Fahrenholz, F. (1995) Alteration of the myometrial plasma membrane cholesterol content with beta-cyclodextrin modulates the binding affinity of the oxytocin receptor. *Biochemistry* **34,** 13784–13793
71. Bosch, B., Grigorov, B., Senserrich, J., Clotet, B., Darlix, J. L., Muriaux, D., and Este, J. A. (2008) A clathrin-dynamin-dependent endocytic pathway for the uptake of HIV-1 by direct T cell-T cell transmission. *Antiviral Research* **80,** 185–193
72. Wang, L. H., Rothberg, K. G., and Anderson, R. G. (1993) Mis-assembly of clathrin lattices on endosomes reveals a regulatory switch for coated pit formation. *J. Cell Biol.* **123,** 1107–1117
73. Rothberg, K. G., Heuser, J. E., Donzell, W. C., Ying, Y. S., Glenney, J. R., and Anderson, R. G. (1992) Caveolin, a protein component of caveolae membrane coats. *Cell* **68,** 673–682
74. Cheng, Z. J., Singh, R. D., Holicky, E. L., Wheatley, C. L., Marks, D. L., and Pagano, R. E. (2010) Co-regulation of caveolar and Cdc42-dependent fluid phase endocytosis by phosphocaveolin-1. *J. Biol. Chem.* **285,** 15119–15125
75. Feng, X., Huang, H., Yang, Y., Fröhlich, O., Klein, J. D., Sands, J. M., and Chen, G. (2009) Caveolin-1 directly interacts with UT-A1 urea transporter: the role of caveolae/lipid rafts in UT-A1 regulation at the cell membrane. *Am. J. Physiol. Renal Physiol.* **296,** F1514–F1520
76. Murtazina, R., Kovbasnjuk, O., Donowitz, M., and Li, X. (2006) Na+/H+ exchanger NHE3 activity and trafficking are lipid Raft-dependent. *J. Biol. Chem.* **281,** 17845–17855
77. Bullis, B. L., Li, X., Singh, D. N., Berthiaume, L. G., and Fliegel, L. (2002) Properties of the Na+/H+ exchanger protein. Detergent-resistant aggregation and membrane microdistribution. *Eur. J. Biochem.* **269,** 4887–4895
78. Inoue, M., Digman, M. A., Cheng, M., Breusegem, S. Y., Halaihel, N., Sorribas, V., Mantulin, W. W., Gratton, E., Barry, N. P., and Levi, M. (2004) Partitioning of NaP_i cotransporter in cholesterol-, sphingomyelin-, and glycosphingolipid-enriched membrane domains modulates NaP protein diffusion, clustering, and activity. *J. Biol. Chem.* **279,** 49160–49171
79. Hansen, G. H., Niels-Christiansen, L. L., Thorsen, E., Immerdal, L., and Danielsen, E. M. (2000) Cholesterol depletion of enterocytes. Effect on the Golgi complex and apical membrane trafficking. *J. Biol. Chem.* **275,** 5136–5142
80. Li, X., Galli, T., Leu, S., Wade, J. B., Weinman, E. J., Leung, G., Cheong, A., Louvard, D., and Donowitz, M. (2001) Na+-H+ exchanger 3 (NHE3) is present in lipid rafts in the rabbit ileal brush border: a role for rafts in trafficking and rapid stimulation of NHE3. *J. Physiol.* **537,** 537–552